Atomic cascade of K^-p and K^-d atoms and Doppler broadening contribution on x-ray widths

S. Z. Kalantari* and M. Raeisi G.
Department of Physics, Isfahan University of Technology, Isfahan, 84156-83111, Iran
(Received 22 June 2009; published 21 January 2010)

In this article we present a new calculation of the cascade of K^-p and K^-d atoms by the Monte Carlo method. Energy dependence of the collisional cascade processes is taken into account. The x-ray yields due to the radiative transition during the cascade are also calculated. We compare our results with the previous calculations by others and by KEK and DEAR experimental data for K^-p atoms. We have also investigated the kinetic energy distribution of K^-p atoms and the role of Coulomb transition on x-ray yields. Finally, the Doppler broadening contribution on the measured width of x-ray spectra are determined. In order to study the strong interaction in low energies, our results for x-ray yields from K^-p and K^-d atoms can be compared with the forthcoming SIDDHARTA collaboration results.

DOI: 10.1103/PhysRevC.81.014608 PACS number(s): 36.10.Gv, 13.75.Jz, 02.70.Uu

I. INTRODUCTION

When a heavy negative particle ($\mu^-, \pi^-, K^-, \ldots$) enters a hydrogen isotope target, an exotic hydrogen atom is formed. The particle may replace an atomic electron, thus becomes bounded in high-n atomic Bohr orbit around the nucleus. The principal quantum number of this highly excited state is of the order $n \simeq \sqrt{m/m_e}$, where m and m_e are the masses of the particle and electron, respectively [1–3]. The exotic atoms formation is followed by an atomic cascade consisting of a multistep transition to lower atomic states. It is a complicated interplay of competitive collisions and radiative deexcitation processes [1–6].

Muonic atoms of hydrogen isotopes are the simplest among the exotic atoms. Muons, in contrast to the other possible particles, are not affected by the strong interaction. So they may serve as the best probe for the investigation of these deexcitation processes.

Studies the other exotic atoms such as K^-p, K^-d, and π^-p are very important in investigating QCD in low energies and strong interaction [5,7–9]. In order to determine the strong interaction component of the kaon-nucleus interaction in low energies, the shift of the K_α energy from the pure electromagnetic calculation energy are measured. The energy levels of kaonic atoms have also a finite absorption width due to the strong interaction between the kaon and nucleus. Thus it is expected that the shift and width of the $1s$ state can be determined by measuring the energy of the K-series x-ray.

For example, for kaonic hydrogen, the $1s$ shift and width can be related to the real and imaginary parts of the K^-p scattering length a_{Kp} by the Deser-Trueman formula [9],

$$\Delta E_{1s} + \frac{i}{2}\Gamma_{1s} = 2\alpha^3\mu^2 a_{Kp}^s = 412\,\text{eV fm}^{-1} a_{Kp}^s, \qquad (1)$$

where $\Delta E_{1s} = (E_{k_\alpha})_{\text{exp}} - (E_{k_\alpha})_{\text{em}}$, μ is the reduced mass of the K^-p system and α is the fine structure constant.

The basic cascade processes are collisional and radiative deexcitation. The known collisional deexcitation processes are external Auger effect, Stark mixing, Coulomb transition, and elastic scattering. A simple kinetics for cascade of muonic hydrogen atoms was discussed by Menshikov [10], and then the kinetics of cascade was developed by Markushin [2,3].

The Coulomb deexcitation [11], is an important accelerating mechanism to produce hot kaonic atoms. The exotic atoms are decelerated by elastic scattering. The evolution of the kinetic energy distribution during the atomic cascade is very important because the rates of collisional processes are energy dependent. The kinetics of the cascade was calculated in a Monte Carlo approach by Markushin [2]. The extended standard cascade model (ESCM) that is presented in Refs. [3,4] introduces some important improvements compared to the earlier models. In this article we also take into account the energy dependence of collisional processes but we do not use any tuning parameters in the Coulomb transition and Stark mixing cross sections. Then the role of the high kinetic energy component of kaonic hydrogen from Coulomb transition on x-ray yields and Doppler broadening contribution on the measured width of x-ray yields are calculated.

The strong interaction shifts and widths affect the absorption during the cascade and therefore the x-ray yields [5,12–14]. Since the calculated x-ray yields from our simulation are confirmed by the existing experimental results for muonic deuterium atoms [6,15], we have developed our Monte Carlo simulation for kaonic hydrogen and deuterium. For this purpose, the cross sections of the cascade processes for kaonic atoms should be calculated in order to be used as an input of our computer code. Our results for x-ray yields of kaonic hydrogen are compared with other simulations [5,12–14] and the two existing measurements in KEK [16] and LNF (DEAR Collaborations) [17].

Until now the x-ray yields of K^-d atoms have not been measured, therefore we can use Γ_{1s} and Γ_{2p} as free parameters in our calculations. The SIDDHARTA (Silicon Drift Detectors for Hadronic Atoms Research by Timing Application) collaboration at LNF in Italy have prepared an experiment to detect precisely the x-ray from K^-d atoms [18]. The experiment have been installed in the DAΦNE machine at LNF recently. Hence, in order to study the strong interaction at low energies, our results for x-ray yields from K^-d atoms can

*Corresponding author: zafar@cc.iut.ac.ir

be compared with the forthcoming SIDDHARTA experimental results. In this article the time dependence of population of excited levels of the kaonic atoms during the cascade are also investigated and the dependence of the deexcitation average time (average cascade time) on the target density (ϕ) are presented.

II. CASCADE PROCESSES OF KAONIC HYDROGEN AND DEUTERIUM

When negative kaon, K^-, is injected into a mixture of hydrogen isotopes it slows down and immediately gets captured into atomic orbits with the size of the electron Bohr radius. So the cascade starts from a highly excited state with a principal quantum number $n \sim \sqrt{m_k/m_e} \approx 25$. The subsequent process is a complicated interplay of competitive collisional and radiative deexcitation processes, which comes to an end by the absorption of the kaon by nucleus or the weak decay of kaon. The cascade processes and their rates (λ) can be summarized as follows:

(1) Radiative transition:

The excited kaonic atoms can be deexcited by spontaneous emission,

$$(K^- x)_{n_i l_i} \to (K^- x)_{n_f l_f} + \gamma, \tag{2}$$

where $x = p, d$ and $n_i l_i$ and $n_f l_f$ are initial and final principal and orbital angular-momentum numbers, respectively. The rate of radiative transition is given by quantum mechanical calculations with electric dipole approximation:

$$\lambda_{\text{rad}}^{n_i l_i \to n_f l_f} = \frac{4}{3}\alpha\mu^{-2}\left(R_{n_f l_f}^{n_i l_i}\right)^2 \frac{\text{Max}(l_i, l_f)}{2l_i + 1}(\Delta E_{if})^3 \qquad n_i < n_f, \quad l_f = l_i \pm 1, \tag{3}$$

where μ is the reduced mass of the kaonic atom, ΔE_{if} is the transition energy and $R_{n_f l_f}^{n_i l_i}$ is the radial matrix elements of hydrogen atom [1]. The radiative transition rate is decreased by increasing n_i.

The known collisional deexcitation processes are chemical dissociation, external Auger effect, Stark mixing, and Coulomb deexcitation. The rates for the collisional transitions depend on target density and the kinetic energy of the exotic atom.

(2) Chemical dissociation:

If $\Delta E_{if} > 4.7$ eV (4.7 eV is the dissociation energy of H_2 molecules) the excited kaonic atom can dissociate the target molecules:

$$(K^- x)_{n_i l_i} + X_2 \to (K^- x)_{n_f l_f} + X^+ + X^-, \tag{4}$$

where $X = H, D$. Leon and Bethe [1] have estimated the cross section for this process to be $\sigma_{\text{chem}} = \frac{1}{2}\pi a_n^2$, where a_n is nth Bohr orbit of the exotic atom. Therefore the rate of chemical dissociation is given by:

$$\lambda_{\text{chem}}^{n_i l_i \to n_f l_f} = \frac{N}{2} v_i \pi a_n^2 \ , \quad l_f = l_i, \tag{5}$$

where N is density of the target and v is the relative velocity of $K^- x$ and the target atoms. This process is important for high initial excitation level n.

(3) External Auger effect:

If excitation energy of $K^- x$ atom is enough to ionize the target molecules, Auger deexcitation can take place. In this process the excitation energy of the kaonic atom is absorbed by an electron of the colliding molecule, then the molecule becomes ionized and an Auger electron is released:

$$(K^- x)_{n_i l_i} + X_2 \to (K^- x)_{n_f l_f} + e^- + X_2^+. \tag{6}$$

The rate of external Auger deexcitation has been calculated by Lone and Bethe [1] in the Born approximation as follows:

$$\lambda_{\text{Aug}}^{n_i l_i \to n_f l_f} = \frac{16}{3} N \mu^{-2}\left(R_{n_f l_f}^{n_i l_i}\right)^2 \frac{\text{Max}(l_i, l_f)}{2l_i + 1}(2\Delta E + 1.39)^{-1/2}, \tag{7}$$

where $\Delta E = \Delta E_{if} - 15.2$ eV (15.2 eV is the ionization energy of H_2 molecules). As usual, the dipole radiation is subject to selection rule $\Delta l = l_f - l_i = 1$. There, a critical level n_c exists, which is the greatest n for which the released binding energy in the $\Delta n = 1$ transition can ionize the target molecule ($\Delta E_{if} > 15.2$ eV). For $n > n_c$ only the transitions with $\Delta n > 1$ are energetically allowed. The Auger rates increase with n_i until it reaches n_c, then on average the Auger rates decrease with n_i.

(4) Stark mixing:

The neutral $K^- x$ can penetrate deep into the target molecule or atom where the electric field mixes the sublevels with the same n. The electric field splits the energy levels and induces oscillation among the resulting n^2 sublevels.

$$(K^- x)_{n_i l_i} + X \to (K^- x)_{n_f l_f} + X, \quad n_f = n_i, l_f \neq l_i \tag{8}$$

The Stark transition affect the population of the nl sublevels. It is especially important as it results in strong absorption during the cascade by feeding the ns states. This effect contributes to the overall deexcitation time.

Those radiative transitions that are primarily forbidden may also become allowed by Stark mixing.

The first detailed calculations of Stark cross sections appeared in an article by Leon and Bethe [1]. They analyzed this problem by means of the rotating field model. A unified framework for calculating Stark mixing, elastic scattering, and nuclear absorption during collisions have also been presented as the close-coupling model by Jensen and Markushin [3].

In this article for the rate of this process we have used the extended method of Borie and Leon [19] formulated by Terada and Hayano [12]. In this method one can consider all of the l transitions in any m quantum number.

(5) Coulomb deexcitation:

The mechanism of this process is similar to stark mixing; when the neutral $K^- x$ approaches a target atom, a much stronger field is needed to mix states with different values of n,

$$(K^- x)_{n_i l_i} + X \to (K^- x)_{n_f l_f} + X. \tag{9}$$

Contrary to Auger transition, where the transition energy of $K^- x$ atom is completely carried away by an electron. In this process the released binding energy is shared between the colliding particles. It is an important acceleration mechanism that produces high kinetic energy kaonic atoms. Bracci and Fiorentini [11] calculated the Coulomb cross section for $\mu^- p$

atoms in the semiclassical approximation. Here we use the same procedure to calculate the Coulomb transition rate for K^-p and K^-d atoms,

$$\lambda_{\text{Coul.}}^{n_i l_i \to n_f l_f} = \frac{N v_i}{4} \pi a_{n_i}^2 \left(1 + \frac{\mu}{E_i n_i^2}\right), \quad n_f = n_i - 1, \quad l_f = l_i, \tag{10}$$

where E_i is the initial kinetic energy of K^-x atom. Transitions with $\Delta n = 1$ dominate and the cross sections were found to grow with increasing n.

(6) Elastic scattering:

In this collisional process the nl states of kaonic atom is not changed where $n_i l_i = n_f l_f$,

$$(K^-x)_{n_i l_i} + X \to (K^-x)_{n_i l_i} + X. \tag{11}$$

This process leads to deceleration of kaonic atoms. Menshikov and Ponomarev estimated the effective rate by the following formula [20]:

$$\lambda_{\text{scat}}^{n_i l_i \to n_f l_f} = N v_i \pi^2 \frac{2 M_{K^-x} M_H}{(2M_{K^-x} + M_H)^2} \frac{n_i^2 - 1}{4 \mu E_i}. \tag{12}$$

(7) Nuclear reaction:

In kaonic atoms, nuclear reactions occur due to the overlap of the k^- and x (p or d) wave functions. The strong interaction leads to a broadening of the $n_i p \to n_f s$ and $n_i d \to n_f p$ x-ray lines. One of the channels of this reaction is given by

$$(K^-x)_{n_i l_i} \to \pi^o + \Lambda. \tag{13}$$

The n dependence of the rates of this process from ns and np states are given by [1],

$$\lambda_{\text{abs}}^{ns} = \frac{\lambda^{1s}}{n^3}, \quad \lambda_{\text{abs}}^{np} = \frac{32}{3} \frac{n^2 - 1}{n^5} \lambda_{\text{abs}}^{2p}, \tag{14}$$

where $\lambda_{\text{abs}} = \Gamma_{\text{abs}}/\hbar$ and Γ_{abs} is the strong absorption width that is determined by experimental values or, theoretically, by solving a Klein-Gordon equation with relevant optical potential [5,22]. Otherwise, they are treated as a parameter.

(8) Nuclear absorption:

Contrary to the nuclear reaction, this process may take place in collision with target atoms. For example, one channel of this process is as follows:

$$(K^-x)_{n_i l_i} + X \to \pi^o + \Lambda + X. \tag{15}$$

Jensen and Markushin included this process in cascade simulations in a close-coupling method by adding an imaginary part to the Coulomb potential for levels $n < 5$ [3,21]. We also used the cross sections calculated by Jensen and Markushin for nuclear absorption in our simulation. The values of cross sections are less than the nuclear reaction cross sections.

The rates of the cascade processes [Eqs. (2)–(15)] are in the atomic unit given by $m_e = \hbar = e = 1$. It should be noted that the kaon may decay in any time,

$$\lambda_{\text{decay}} = 8.13 \times 10^7 \text{ s}^{-1}. \tag{16}$$

The collisional deexcitations dominate at the beginning of the cascade that is related to the highly n states, whereas deexcitations from lower n states to the ground state are mostly radiative. During the atomic cascade a large fraction of the atoms are not thermalized [2,23–25]. Some experimental evidence for the high-velocity components exist for π^-p atoms [26,27], which are related to the Coulomb transitions.

III. MONTE CARLO SIMULATION OF THE KAONIC ATOM CASCADE DYNAMICS

Kinetics of the cascade processes of exotic atoms can be studied by solving the kinetics equations [5,6,12,28,29]. The energy dependence of the cross sections is not usually taken into account by this method; however, this can be considered by a multigroup method [6,29]. But Monte Carlo simulation is the most powerful method for taking into account all the parameters such as time and energy dependence of the collisional cascade processes in the investigation of the exotic atom cascade dynamics. We can also calculate the x-ray yields from radiative transition (especially K_α, K_β, and K_γ) by the Monte Carlo simulation. For this purpose we have prepared a computer code based on the Monte Carlo method. The cross sections and rates of the cascade processes given by Eqs. (2)–(16) should be calculated numerically to be used as input for our computer code.

The program starts from a highly excited state of exotic atoms ($n_i \sim 25$ for kaonic hydrogen and deuterium and l_i is distributed statistically [3]). The life history is followed step by step during the cascade through nl states. For this purpose the transition probability from $n_i l_i$ to $n_f l_f$ due to any jth processes (2)–(10) in the initial kinetic energy E_i, $P_j^{n_i l_i \to n_f l_f}(E_i)$, should be determined before any step of deexcitation. This probability is given by:

$$P_j^{n_i l_i \to n_f l_f}(E_i) = \frac{\lambda_j^{n_i l_i \to n_f l_f}(E_i)}{\lambda_{\text{tot}}^{n_i l_i}(E_i)}, \tag{17}$$

where, $\lambda_{\text{tot}}^{n_i l_i}(E_i)$ is the total transition rate from excited state $n_i l_i$ and it is given by the following expression:

$$\begin{aligned} \lambda_{\text{tot}}^{n_i l_i}(E_i) = & \sum_{n_f=1}^{n_i-1} \lambda_{\text{chem}}^{n_i l_i \to n_f l_i}(E_i) + \sum_{n_f=1}^{n_i-1} \sum_{l_f=0}^{n_f-1} \lambda_{\text{rad}}^{n_i l_i \to n_f l_f} \delta_{l_i \pm 1, l_f} \\ & + \sum_{n_f=1}^{n_i-1} \sum_{l_f=0}^{n_f-1} \lambda_{\text{Aug}}^{n_i l_i \to n_f l_f} \delta_{l_i \pm 1, l_f} + \sum_{l_f \neq l_i}^{n_i-1} \lambda_{\text{Stark}}^{n_i l_i \to n_i l_f}(E_i) \\ & + \sum_{n_f=1}^{n_i-1} \lambda_{\text{Coul.}}^{n_i l_i \to n_f l_i}(E_i) + \lambda_{\text{nul.-re}}^{n_i l_i} + \lambda_{\text{abs}}^{n_i l_i}(E_i) \\ & + \lambda_{\text{scat.}}^{n_i l_i \to n_i l_i}(E_i) + \lambda_{\text{decay}}, \end{aligned} \tag{18}$$

where δ_{ij} is Kronecer delta.

By the Monte Carlo method we can then determine the type of the cascade processes and final state $n_f l_f$ of kaonic atom in any step. The program also determines the final kinetic energy E_f of exotic atoms after any collisional processes such as Coulomb deexcitation, elastic scattering, Stark mixing, and Auger effect in each step. To calculate the kinetic energy of exotic atoms after any collision with atoms or molecules of the target we have used the method of Sachs and Teller [30] that is also explained in Ref. [31]. The cascade time is also calculated using the rates of the reactions.

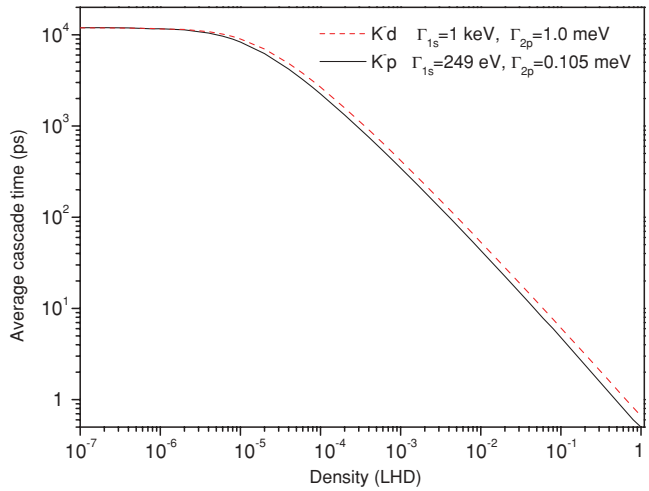

FIG. 1. (Color online) Average cascade time of kaonic atoms as a function of target density. Solid line for $K^- p$ atoms and dashed line for $K^- d$ atoms.

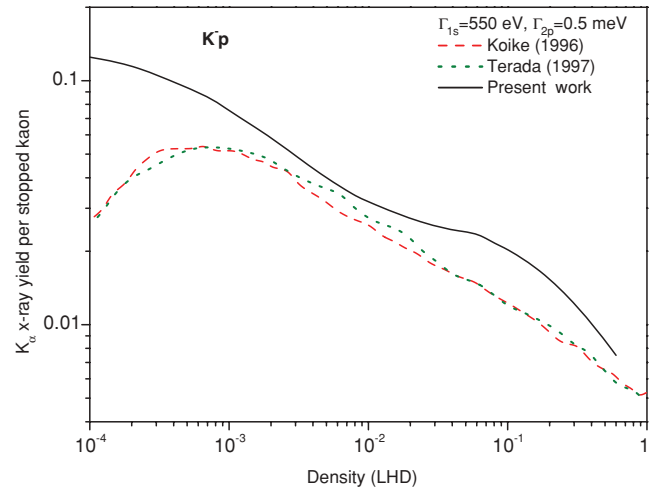

FIG. 2. (Color online) Comparison of the present density dependence of K_α x-ray yield (solid line) with the Koike [5] (dashed line) and Terada [12] (dotted line) works for $K^- p$ atoms.

At any interval time we determine the state of the kaonic atom until it reaches to the ground state or it is absorbed by the nucleus or the kaon decay. This procedure is repeated for 10^6 kaonic atoms; then the number of any event in any time interval is computed during the atomic cascade. We determine the average values of the significant parameters such as the average cascade time, the population of the kaonic atoms in any state n as a function of time, normalized kinetic energy distribution of $K^- p$ and $K^- d$ atoms, and x-ray yields per stopped kaon in the target. Figure 1 shows the average cascade time for $K^- p$ and $K^- d$ atoms as function of target density (ϕ). It shows the average transition time is decreased by increasing the density (ϕ). In fact, if the density of the target is increased, the collisional cascade processes [given by Eqs. (3)–(12) and (15)] increase, since the collisional processes are much faster than the radiative transition. Therefore when ϕ is increased the cascade time is decreased.

IV. X-RAY YIELD OF $K^- p$ ATOMS

The strong interaction shifts and widths affect the number of absorption events during the cascade and therefore the x-ray yields [5,13–15]. During the cascade of $K^- p$ atoms, radiative transition may take place which is more important in the lower states. In the Monte Carlo simulation of the atomic cascade, the program follows the story of 10^6 kaon which are stopped in the hydrogen target and records the number of x-ray with its energy (for example K series). Then the x-ray yields per stopped kaon at different target densities are computed.

Initially we compare our results with the cascade calculations that were already presented by Terada [12] and Koike [5]. We have used the rates of the radiative transition, chemical dissociation, Auger effect, and nuclear absorption from the same expression that have been used by Terada and Koike. For Stark mixing we have used the extended method of Borie and Leon [19] formulated by Terada [12], because it gives more completed rates of Stark mixing with no need to tune a the free parameter $k_{\rm stk}$. Koike [5] used the Borie and Leon method for Stark mixing rates in cascade calculations. It should be noted that in the Koike and Terada cascade calculations the Coulomb deexcitation, elastic scattering, and absorption [Eq. (8)] is not taken into account and kinetic energy of the $K^- p$ atoms is considered as a constant parameter ($E_k = 1$ eV). However, we have considered all of the cascade processes [Eqs. (2)–(16)] and the energy dependence of the collision rates [Eqs. (3)–(12) and (15)]. Furthermore, our method of cascade calculation is different from the one used in Refs. [5,12]. In fact, we have used the Monte Carlo method, whereas Kioke and Terada have used the kinetics equations and the matrix calculation to solve them.

In Figs. 2–4 we have compared our results with the x-ray yields for $K^- p$ atoms that were calculated by Koike [5] and Terada [12] at different densities. They used the nearly

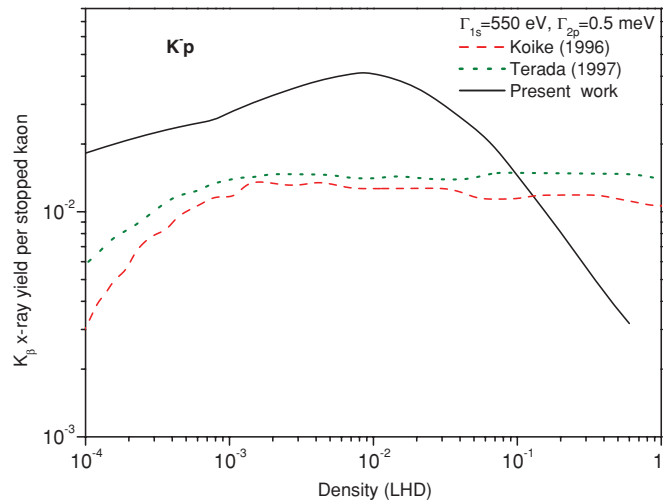

FIG. 3. (Color online) Comparison of the present density dependence of K_β x-ray yield (solid line) with the Koike [5] (dashed line) and Terada [12] (dotted line) works for $K^- p$ atoms.

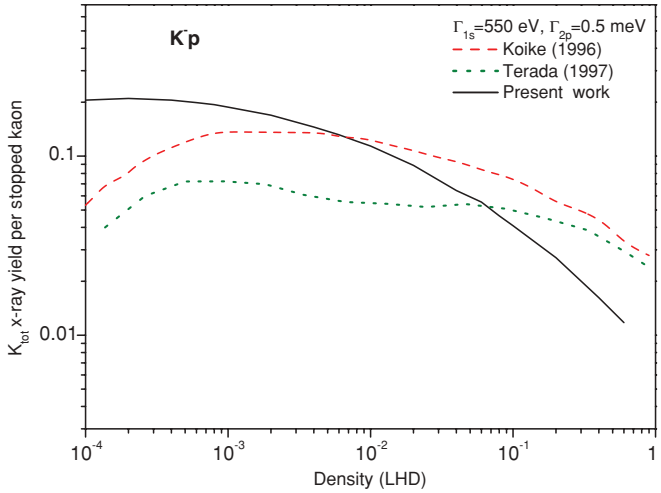

FIG. 4. (Color online) Comparison of the present density dependence of K_{tot} x-ray yield (solid line) with the Koike [5] (dashed line) and Terada [12] (dotted line) works for K^-p atoms.

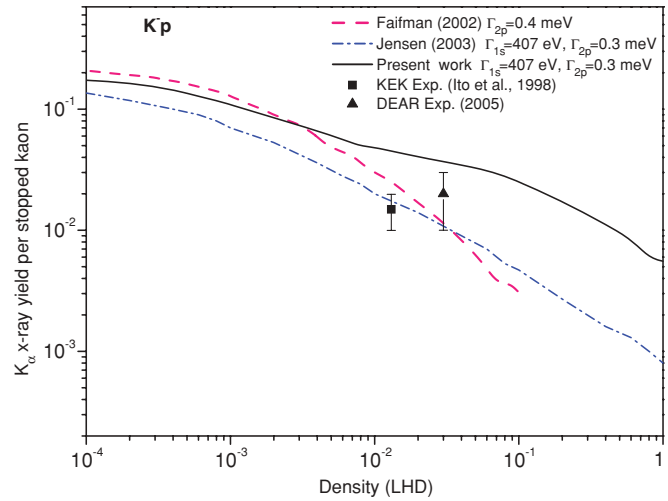

FIG. 5. (Color online) Comparison of the present density dependence of K_α x-ray yield (solid line) with the Faifman [13] (dotted line) and Jensen [14] (dashed-dotted line) works for K^-p atoms. The experimental results from KEK [16] and DEAR [17] have also been shown.

average of the theoretical values for $|\Delta E_{1s}| = 300\,\text{eV}$ and $\Gamma_{1s} = 550\,\text{eV}$ and they considered Γ_{2p} as a free parameter. In order to compare our method with Refs. [5,12], our present work has also been carried out with the same Γ_{1s} and Γ_{2p} ($\Gamma_{2p} = 0.5\,\text{meV}$). Figures 2–4 show that the x-ray yields decrease with density. At higher densities the probability of the collisions among Stark mixing is enhanced. Stark mixing leads to an increase in the population of the s and p states, where nuclear reaction and absorption take place faster specially at ns states. Therefore we expect that this decreasing behavior at high densities is established for all the K-series x-rays. Figure 2 shows this decreasing variation for K_α x-ray yield in the present work and as well as for two other calculations (Koike and Terada); however, for K_β x-ray yields, only our calculation shows this expected variation with respect to density (Fig. 3). In other words K_β x-ray yields in Koike and Terada calculations are approximately constant in high densities. However, our calculation shows the decreasing variation for K_β yields in the high densities.

More recent and complete cascade calculations for K^-p atoms have been carried out by Jensen and Markushin [3,14,32] and Faifman [13]. They also considered the energy dependence of the cascade rates in their cascade calculations by the ESCM. In Figs. 5 and 6 we have also compared our x-ray results for K^-p atoms with the Jensen [14] and Faifman [13] results. The curves from the Jensen's work is related to $\Delta E_{1s} = 323\,\text{eV}$ and $\Gamma_{1s} = 407\,\text{eV}$ that have been extracted from the KEK measurement [16] and $\Gamma_{2p} = 0.3\,\text{meV}$ assuming. In order to compare with the results of Ref. [14], we are using the same Γ_{1s} and Γ_{2p} parameters in Figs. 5 and 6. However, more precise measurement by DEAR (DAϕNE Exotic Atom Research) collaboration [17] gives $\Delta E_{1s} = -193 \pm 37(\text{stat}) \pm 6(\text{syst})\,\text{eV}$ and $\Gamma_{1s} = 249 \pm 111(\text{stat}) \pm 30(\text{syst})\,\text{eV}$. Figure 5 shows that our K_α x-ray yields have approximately the same order of magnitude of the results given in the two other works in low densities ($\phi < 5 \times 10^{-3}$ of LHD)[1], but it is greater in higher densities. Jensen has chosen $\Gamma_{2p} = 0.3\,\text{meV}$ [32] to obtain a better fit with the KEK data at $\phi = 0.013$ of LHD. Figure 5 shows that the Jensen curve is closer to the KEK [16] data in comparison to our curve. But it could be a direct consequence of using not accurate values for Γ_{1s} and Γ_{2p} for which we have used the Jensen's choice. In fact, in our calculation we should choose a more precise measurement for 1s width ($\Gamma_{1s} = 249\,\text{meV}$) by DEAR collaboration and a better fitting is needed to determine the

[1]LHD is liquid hydrogen density, which is equal to $4.25 \times 10^{22}\,\frac{\text{atoms}}{\text{cm}^3}$.

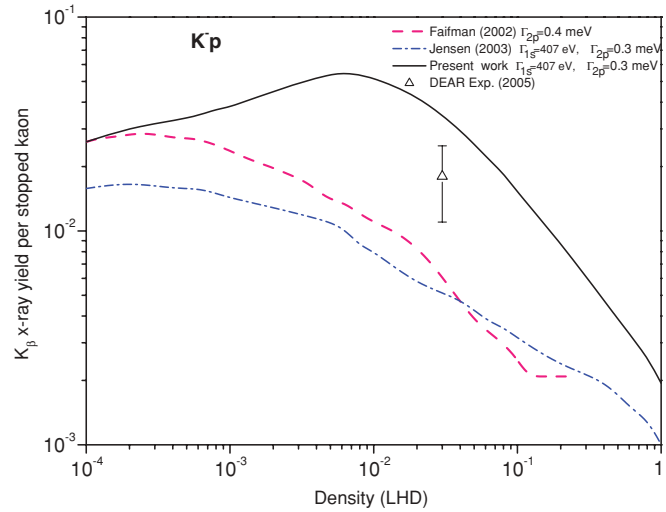

FIG. 6. (Color online) Comparison of the present density dependence of K_β x-ray yield (solid line) with the Faifman [13] (dotted line) and Jensen [14] (dashed-dotted line) works for K^-p atoms. The experimental result from DEAR [17] have also been shown.

Γ_{2p} value. However, all of the incident kaons in the target do not succeed to form kaonic atoms. Some of them decay before stopping and some of them escape from the target. Therefore, to compare our results correctly with the experimental values, we should calculate the x-ray yields per incoming kaon to the target instead of per stopped kaon. It can be calculated if the values of the x-ray yields per stopped kaon (Figs. 5 and 6) are multiplied by the values of kaonic atom formation probability [33].

Figures 5 and 6 show that the values of K_α and the values of K_β from our results are greater than the existing experimental data. However, the values from Refs. [13,14] are less than the DEAR experimental data point that is a more precise experiment on x-ray yields. Therefore if the calculated x-ray yields per stopped kaon multiplies the kaonic atom formation probability (which is less than 1 [33]), our calculated values for K_α and K_β per incoming kaons approach to the experimental values. However, the two other calculated results from Refs. [13,14] become smaller in value.

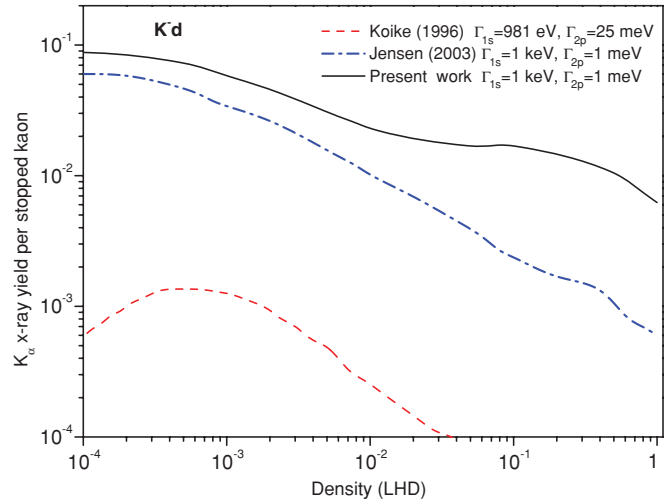

FIG. 7. (Color online) Comparison of the present density dependence of K_α x-ray yield (solid line) with the Koike [5] (dashed line) and Jensen [14] (dashed-dotted line) works for K^-d atoms.

V. X-RAY YIELD OF K^-d ATOMS

The x-ray yields of K^-d atoms have not been measured yet. However, the SIDDHARTA Collaboration is planned to detect precisely the x-ray yields to measure the $1s$ strong interaction shift and width in kaonic deuterium for the first time [18,34]. Therefore cascade calculation for prediction of the absolute x-ray yields is important. Since the x-ray of K^-d atoms are rare, calculating the K^-d atom x-ray yields as a function of target density is very important for choosing the optimum density in the corresponding experiment setups [33]. Furthermore, these calculations are useful in data analysis.

For this purpose we have repeated the calculations of the rates of the cascade processes of K^-p atoms for K^-d atoms [Eqs. (2)–(15)]. Calculation of nuclear absorption rates [Eq. (15)] for K^-d atoms has not been carried out yet, therefore we have used the values for K^-p atoms [3,21] for these rates. Then using the same procedure explained in the previous section, the cascade of K^-d atoms is simulated by the Monte Carlo method and the x-ray yields per stopped kaon have been computed as a function of density. The values of ΔE_{1s}, Γ_{1s}, and Γ_{2p} for K^-d atoms have not been measured yet. However, there exist some theoretical estimated values [5,22]. In order to make an easy comparison with Jensen's work [14,32], we have considered the same values as Jensen ($\Delta E_{1s} = 0.5$ keV, $\Gamma_{1s} = 1$ keV, and $\Gamma_{2p} = 1$ meV). Figures 7 and 8 show that the variation of K^-d x-ray yields vs. density is almost similar to the K^-p x-ray yields. Like K^-p atoms the yields for K^-d atoms are larger than Jensen and Koike works. This increases the chance for a successful SIDDHARAT experiment. In the diluted gas target the K^-p stopping power is low and the decay of kaon dominates, therefore by using Fig. 7 higher densities near 0.1 of LHD are suggested to have the appropriate x-ray.

Finally, we present a suggestion for the SIDDHARTA experiment: x-ray measurement for K^-p and K^-d in different densities are needed to determine Γ_{1s} and Γ_{2p} parameters. If we get the suggested results, we can take Γ_{1s} and Γ_{2p} as free parameters; then they can be determined by fitting the simulated x-ray curves (as a function of density) with the experimental curves.

VI. INVESTIGATION OF THE KINETIC ENERGY DISTRIBUTION OF K^-p ATOMS

If the kinetic energy distribution of K^-p atoms is calculated in some nl states, the important role of Coulomb deexcitation to produce the high-energy component of K^-p atoms can be seen. Figure 9 shows the average kinetic energy distribution in $2p$ state. It shows the peaks at energies 473.7, 165.8, and 76.7 eV that are produced by the $3 \to 2$, $4 \to 3$, and $5 \to 4$, Coulomb transition, respectively. Figure 9 shows that the ki-

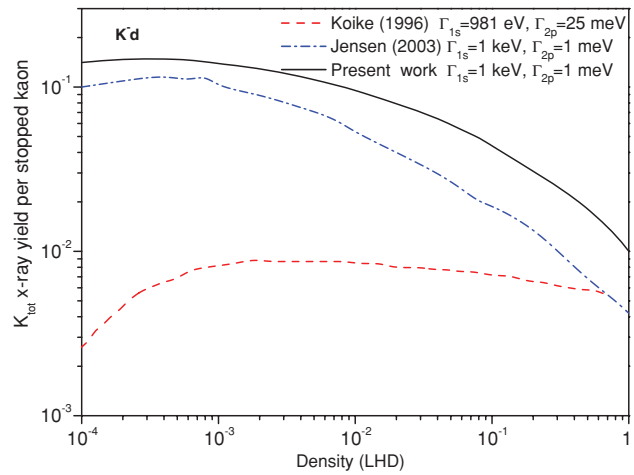

FIG. 8. (Color online) Comparison of the present density dependence of the $K_{\rm tot}$ x-ray yield (solid line) with the Koike [5] (dashed line) and Jensen [14] (dashed-dotted line) works for K^-d atoms.

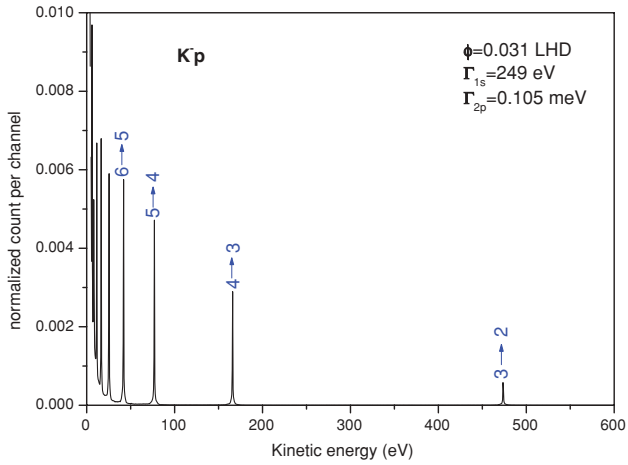

FIG. 9. (Color online) Kinetic energy distribution of K^-p atoms in $2p$ state.

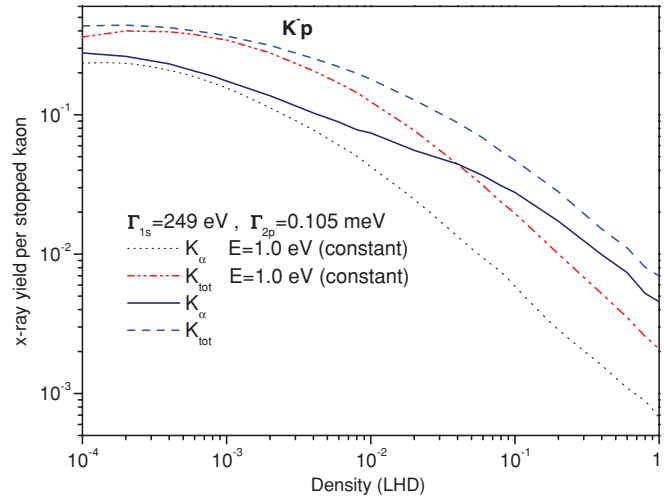

FIG. 10. (Color online) Comparison of the x-ray yield per stopped kaon in two cases, with considering constant kinetic energy and without considering constant kinetic energy of K^-p atoms.

netic energy distribution of K^-p atoms in $2p$ state depends not only on the $3 \rightarrow 2$ Coulomb transition but also on the higher Coulomb transitions such as $4 \rightarrow 3$ and $5 \rightarrow 4$ and so on. Because, the K^-p atoms that go through the $4 \rightarrow 3$ Coulomb transitions, may gain the 165.8 eV kinetic energy in $3d$ state, so they can go through the $3d \rightarrow 2p$ radiative transition without losing kinetic energy. Thus, K^-p atoms in $2p$ state appear with the 165.8 eV kinetic energy by $4 \rightarrow 3$ Coulomb transitions. Likewise, the $5 \rightarrow 4$ Coulomb transitions can contribute to the kinetic energy distribution of K^-p atoms in the $2p$ state.

A. Sensitivity of the x-ray yields to the kinetic energy distribution of K^-p atoms

In this section we compare the calculated x-ray yields of K^-p atoms in two cases:

(i) Kinetic energy of K^-p atoms is considered a constant parameter ($E_k = 1.0\,\text{eV}$).
(ii) Kinetic energy of K^-p atoms is not considered constant and we take into account its evolution by accelerating (Coulomb deexcitation) and decelerating (elastic scattering and stark mixing) processes.

Figure 10 shows that if we consider the kinetic energy evolution during the cascade of K^-p atoms, the calculated x-ray yields are greater than the x-ray results for constant kinetic energy. The difference between the x-ray results in the two cases increases with density, because in the higher densities the collisional processes that are energy dependent are more probable. Figure 10 shows this fact is important in the densities higher than $\varphi = 0.001$ of LHD. For example at $\varphi = 0.1$ of LHD, the calculated K_α in the second case (considering the kinetic energy evolution) is approximately 4.3 times greater than its calculated value in the first case (considering the constant kinetic energy) and it is approximately 2.5 times greater than for K_{tot}. It shows that the evolution of kinetic energy distribution during the cascade dynamics is very important to calculate the x-ray yields.

B. Doppler broadening effect on the measured width of x-ray yields

The kinetic motion of the K^-p atoms at the instant radiative transitions appears as a Doppler broadening profile in the experimental x-ray spectra [35]. The Doppler broadening due to the high kinetic energy component of K^-p atoms is combined with strong interaction width Γ_{1s}^{had} [Eq. (1)], and makes a convolution profile of the $np \rightarrow 1s$ experimental x-ray lines. In order to extract the strong interaction width for $1s$ state(Γ_{1s}^{had}), the Doppler broadening ($\delta\Gamma_{1s}^{D}$) must be subtracted from the measured width Γ_{1s}^{m} of the x-ray spectra.

$$\Gamma_{1s}^{m} = \Gamma_{1s}^{\text{had}} + \delta\Gamma_{1s}^{D}. \tag{19}$$

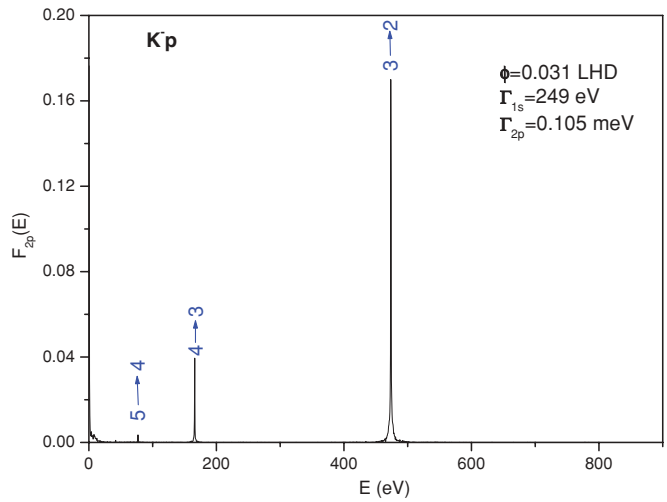

FIG. 11. (Color online) Kinetic energy distribution of K^-p atoms in $2p$ state at the instant of $2p \rightarrow 1s$ radiative transition.

TABLE I. Calculated average Doppler broadening and its contribution on the observed width.

φ (LHD)	$\delta\overline{\Gamma^D_{1s}}$ (eV)	$\overline{\gamma_{2p}}$ (%)
0.031	5.98	2.4
0.100	7.97	3.2
1.00	8.71	3.5

Doppler broadening of the $2p \rightarrow 1s$ radiative transition is determined as follows.

$$\delta\Gamma^D_{1s} = \frac{v}{c} E_{2p\rightarrow 1s}, \tag{20}$$

where v is the velocity of K^-p atoms at the moment of the radiative transition and $E_{2p\rightarrow 1s}$ is the $2p \rightarrow 1s$ radiative transition energy. In order to determine the average Doppler broadening ($\delta\overline{\Gamma^D_{1s}}$) we have calculated the kinetic energy distribution of K^-p atoms in $2p$ state at the instant of $2p \rightarrow 1s$ radiative transition [$F_{2p}(E)$]. Figure 11 shows the contribution of the higher Coulomb transition to produce the high kinetic energy component of K^-p atoms in $2p$ state. The reason was explained in Sec. VI. The average Doppler broadening contribution on the measured $1s$ width is calculated as follows,

$$\delta\overline{\Gamma^D_{1s}} = \frac{\int_0^\infty \delta\Gamma^D_{1s} F_{2p}(E) dE}{\int_0^\infty F_{2p}(E) dE}. \tag{21}$$

For this purpose we have calculated $\delta\Gamma^D_{1s}$ numerically using the simulated results from Fig. 11 for $F_{2p}(E)$. The calculated results for $\delta\Gamma^D_{1s}$ in three different densities have been presented in Table I. $\overline{\gamma_{2p}}$ is the contribution of the $2p \rightarrow 1s$ Doppler broadening on the observed Γ_{1s}, where $\overline{\gamma_{2p}} = \frac{\delta\overline{\Gamma^D_{1s}}}{\Gamma^m_{1s}}$ and Γ^m_{1s} is considered from DEAR experiment [17] ($\Gamma^m_{1s} = 249$ eV). It is very important to extract the $\Gamma^{\rm had}_{1s}$ from experimental results. Thus it should be used to analyze the experimental results such as SIDDHARTA experiment [34].

VII. CONCLUSION

In this article we first presented a Monte Carlo method to calculate the cascade dynamics of K^-p and K^-d atoms, then we compared our results with the other previous calculations.

A. K^-p atoms

Our results for K-series x-ray yields are more comparable with the two other calculations by Faifman [13] and Jensen [14] because they have also taken into account the energy dependence of the collisional processes rates. However, our results for K_α and K_β x-ray yields are greater in high densities.

Our results for x-ray yields per stopped kaon are also greater than the two existing data points for x-ray yields (KEK and DEAR). Thus if our results multiply the kaonic atom formation probability that is less than 1 [33], our calculated values for x-ray K series per incoming kaons approach to the experimental values.

The x-ray yields decrease with density because at higher densities the probabilities of collisions among Stark mixing are enhanced. Stark mixing leads to an increase in the population of the s and p states, where nuclear reaction and absorption take place faster, especially at ns states. While at low densities we expect a decreasing behavior for x-ray yields, as the collisional processes are rare at low densities and so most of the kaonic atoms cannot succeed to reach the lower-n states and radiate x-rays. Actually, kaons decay before they can deexcite to lower-n states by collisional processes. This fact is clearly shown in Fig. 1 where the cascade time approaches to the kaon lifetime at very low densities.

B. K^-d atoms

The x-ray yields of K^-d atoms have not been measured yet. Our calculation shows that variation of K^-d x-ray yields vs. density, is approximately similar to the K^-p x-ray yields, except that in this case the x-ray yields are smaller than those of K^-p atoms due to the larger absorption width. Like K^-p atoms, our yields for K^-d atoms are larger than Jensen's and Koike's works and consequently are more promising for the forthcoming SIDDHARATA experiment. In the diluted gas target the K^- stopping power is low and the decay of kaon dominates; however, the x-ray yields decrease by increasing density. Therefore using Fig. 7, higher densities near 0.1 LHD is suggested to reach higher x-ray yields.

Because we do not have a reliable value for Γ_{2p}, it was taken as a free parameter to determine the order of magnitude of the x-ray yields. We suggest that by experiments in several densities, the values of Γ_{1s} and Γ_{2p} for K^-d and K^-p atoms be determined by fitting the simulated x-ray curves (as a function of density) with the experimental data.

Finally, we investigated the kinetic energy distribution of K^-p atoms. The role of the Coulomb transition on x-ray yields and the Doppler broadening contribution on the measured width of x-ray yields were determined. It was shown that the evolution of kinetic energy distribution during the cascade dynamics by Coulomb transitions is very important to calculate the x-ray yields. We showed that the calculated x-ray yields considering kinetic energy evolution during the cascade are greater than the x-ray results with constant kinetic energy assumption. The difference between the x-ray results in two cases increases with density as depicted in Fig. 10.

The high kinetic energy component of K^-p atoms appear as Doppler broadening profile in the experimental x-ray lines. We have calculated the average Doppler broadening contribution on the observed width in K_α line by using the simulated kinetic energy distribution of K^-p atoms in $2p$ state at the instant of $2p \rightarrow 1s$ radiative transition (Table I). It should be used to extract the $\Gamma^{\rm had}_{1s}$ from experimental results.

ACKNOWLEDGMENTS

The authors thank Professors C. Guaraldo and C. Curceanu-Petrascu for many helpful discussions and for inviting us to LNF and introducing the DEAR and SIDDHARTA experiments.

[1] M. Leon and H. A. Bethe, Phys. Rev. **127**, 636 (1962).
[2] V. E. Markushin, Phys. Rev. A **50**, 1137 (1994).
[3] T. S. Jensen and V. E. Markushin, Eur. Phys. J. D **19**, 165 (2002); Lect. Notes Phys. **627**, 37 (2003).
[4] T. S. Jensen and V. E. Markushin, Eur. Phys. J. D **21**, 271 (2002).
[5] T. Koike, T. Harada and Y. Akaishi, Phys. Rev. C **53**, 79 (1996).
[6] S. Z. Kalantari and M. Raeisi, in *Proceedings of the International Conference on Muon Catalyzed Fusion and Related Topics (μCF-07), 18–21 June 2007, Dubna, Russia*, edited by L. I. Ponomarev *et al.* (Joint Institute for Nuclear Research, Dubna, 2007), p. 245.
[7] A. N. Ivanov *et al.*, Eur. Phys. J. A **21**, 11 (2004); Phys. Rev. A **71**, 052508 (2005).
[8] G. Guaraldo *et al.*, Hyperfine Interact. **119**, 253 (1999).
[9] S. Deser *et al.*, Phys. Rev. **96**, 774 (1954); T. L. Trueman, Nucl. Phys. **26**, 57 (1961).
[10] L. I. Menshikov, Muon Catalyzed Fusion **2**, 173 (1988).
[11] L. Bracci and G. Fiorentini, Nuovo Cimento **213**, 9 (1977).
[12] T. P. Terada and R. S. Hayano, Phys. Rev. C **55**, 73 (1997).
[13] M. P. Faifman and L. I. Menshikov, in *Proceedings of the International Workshop on Exotic Atoms: Future Perspective (EXA02), 28–30 November 2002, Vienna*, edited by P. Kienele *et al.* (Austrian Academy of Science Press, Vienna, 2003), p. 185.
[14] T. S. Jensen, Laboratori Nazionali Di Frascati Report, DEAR Technical Note No. IR-46, 2003.
[15] B. Lauss *et al.*, Phys. Rev. A **60**, 209 (1999).
[16] T. M. Ito *et al.*, Phys. Rev. C **58**, 2366 (1998).
[17] G. Beer *et al.*, Phys. Rev. Lett. **94**, 212302 (2005); C. Curceanu (private communication).
[18] http://www.lnf.infn.it/esperimenti/siddharta/.
[19] E. Borie and M. Leon, Phys. Rev. A **21**, 1460 (1980).
[20] L. I. Menshikov and L. I. Ponomarev, Z. Phys. D **2**, 1 (1986).
[21] T. S. Jensen (private communication).
[22] R. C. Barrett and A. Deloff, Phys. Rev. C **60**, 025201 (1999).
[23] S. Z. Kalantari and V. Tahani, Hyperfine Interact. **142**, 627 (2002).
[24] P. Froelich, Adv. Phys. **41**(5), 405 (1992).
[25] M. Jeitler *et al.*, Phys. Rev. A **51**, 2881 (1995).
[26] D. Gotta, in *Proceedings of the International Conference on Exotic Atoms and Related Topics (EXA05), 21–25 February 2005, Vienna, Austria*, edited by A. Hirh *et al.* (Austrian Academy of Science Press, Vienna, 2005), p. 165.
[27] F. Kottmann *et al.*, Hyperfine Interact. **119**, 3 (1999).
[28] S. Z. Kalantari and M. Sohani, Int. J. Mod. Phys. E **11**, 539 (2002).
[29] S. Z. Kalantari and M. H. Pirahmadian, Iranian J. Phys. Res. **6**, 250 (2006).
[30] R. G. Sachs and E. Teller, Phys. Rev. **60**, 18 (1941).
[31] J. S. Cohen, Phys. Rev. A **34**, 2719 (1986).
[32] T. S. Jensen, in *Proceedings of the DAΦNE 2004: Physics at meson factories, 7–11 June 2004, Frascati, Italy* (LNF, Frascati Physics Series, 2004); http://hal.archieves-ouvertes.fr/docs/00/02/83/57/PDF/Jensen.pdf.
[33] M. Raeisi G. and S. Z. Kalantari, Phys. Rev. A **79**, 012510 (2009).
[34] C. Curceanu (petrascu) *et al.*, Eur. Phys. J. A **31**, 537 (2007); J. Marton *et al.*, in *Proceedings of the International Conference on Muon Catalyzed Fusion and Related Topics (μCF-07), 18–21 June 2007, Dubna, Russia*, edited by L. I. Ponomarev *et al.* (Joint Institute for Nuclear Research, Dubna, 2007), p. 214.
[35] T. S. Jensen, Eur. Phys. J. D **31**, 11 (2004).